Multiphasic Kinetics of Myoglobin/Sodium Dodecyl Sulfate Complex Formation

Alessandro Feis,* Luca Tofani,* Giampiero De Sanctis,† Massimo Coletta,‡ and Giulietta Smulevich*
*Department of Chemistry, Università di Firenze, I-50019 Sesto Fiorentino (FI), Italy; †Department of Molecular, Cellular, and Animal Biology, Università di Camerino, I-62032 Camerino (MC), Italy; and ‡Department of Experimental Medicine and Biochemical Sciences, Università di Roma Tor Vergata, I-00133 Roma, Italy

ABSTRACT We have carried out a kinetic analysis of the conformational changes that myoglobin (Mb) undergoes in the presence of the anionic surfactant sodium dodecyl sulfate (SDS). The time-resolved results have been combined with steady-state circular dichroism (CD) and resonance Raman (RR) spectroscopy. Time-resolved absorption spectra indicate that SDS induces changes in the heme coordination with the formation of three different Mb species, depending on SDS concentration. The formation of the Mb/SDS complex involves three or four phases, depending on surfactant concentration. The kinetic data are analyzed assuming two modes of interaction according to whether SDS is monomeric or micellar. The two pathways are separated but interconnected through free Mb. At the lowest concentrations a six-coordinated, low-spin form dominates. Two distinct five-coordinated species are formed at higher SDS concentrations: one is a protein-free heme and the other reequilibrates slowly with the six-coordinated, low-spin form. The resulting complexes have been characterized by CD and RR. In addition, CD spectra show that the local changes in the heme environment are coupled to changes in the protein structure.

INTRODUCTION

The formation of complexes between proteins and surfactants involves a wide range of interactions, depending on the nature of both components (1,2). Membrane proteins are usually stabilized by surfactant micelles, mainly through hydrophobic interactions similar to those naturally occurring in cell membranes. Soluble proteins can also give rise to protein/surfactant complex formation, which is often accompanied by protein unfolding processes ranging from moderate conformational changes (3) to extended alterations of the secondary and tertiary structure (4). An advantageous model of the latter process is represented by the binding of ionic surfactants to small globular proteins. Mb is an especially suitable protein, since it has intrinsic spectroscopic probes, i.e., its aromatic amino acids and the heme group. In a previous work (5), we found that Mb/surfactant complexes display multiple interaction modes, giving rise to reversible conformational changes which can be interpreted in terms of different degrees of protein unfolding. The combination of electronic absorption, fluorescence spectroscopy, and tensiometry highlighted important aspects of Mb/surfactant interactions. In particular, the addition of sodium dodecyl sulfate (SDS) at submicellar concentrations induced the formation of a heme six-coordinated, low-spin species (6cLS), possibly through distal histidine (His-64) binding. When the concentration was increased, the formation of two different high-spin heme complexes was observed. The spectroscopic measurements were correlated with the surface tension measurements, which allowed the determination of both the critical aggregation concentration (0.37 mM) and the critical micellar concentration (cmc) (4 mM) for Mb/SDS. Formation of 6cLS Mb at SDS submicellar concentration has been subsequently confirmed, and the dynamics of CO rebinding and dissociation has been studied by time-resolved absorption and photoacoustic spectroscopy (6).

In this work, we first focus on the characterization of the three stationary Mb/SDS complexes by circular dichroism (CD) and resonance Raman (RR) spectroscopy. We then extend the study to the dynamics of complex formation and protein unfolding by time-resolved absorption spectroscopy. We observe different modes of interaction depending on the surfactant concentration, i.e., on the aggregation state of the surfactant. The kinetics can be modeled on the basis of two parallel pathways, which include both the three species observed by steady-state spectroscopy and additional reaction intermediates, which cannot be detected under equilibrium conditions.

MATERIALS AND METHODS

Materials

Horse Mb was purchased from Biozyme (Reinheitszahl = 4.8) (San Diego, CA) or Sigma (St. Louis, MO) (Reinheitszahl = 5.2) and used without further purification. The protein was dissolved in 4-morpholinepropanesulfonic acid (Boehringer Mannheim, Ingelheim am Rhein, Germany) buffer solution at 20 mM concentration and pH 7 for all the experiments except CD spectroscopy in the 200–250 nm region, where a 10 mM buffer at pH 7.2 was used. The complex Mb-imidazole was obtained in 100 mM Tris(hydroxymethyl)aminomethane-HCl buffer, pH 8. The solutions were filtered with Millex SV filters (Millipore, Billerica, MA) before use. The concentration of the protein, determined spectrophotometrically using $\varepsilon = 157\ \mathrm{cm}^{-1}\ \mathrm{mM}^{-1}$ at 409 nm (7), was 11 μM for the CD measurements in the

Submitted November 9, 2006, and accepted for publication January 22, 2007.

Address reprint requests to Giulietta Smulevich, Tel.: 39-055-4573083; Fax: 39-055-4573077; E-mail: giulietta.smulevich@unifi.it.

Luca Tofani's present address is Menarini Ricerche S.p.A., Via Sette Santi 3, I-50131 Firenze, Italy.

© 2007 by the Biophysical Society

0006-3495/07/06/4078/10 $2.00

doi: 10.1529/biophysj.106.100693

250–500 nm region, 5 μM for the CD measurements in the 200–250 nm region, 60–90 μM for RR spectroscopy, and 3 μM for the kinetic measurements. SDS (99% purity) and imidazole were purchased from Merck (Darmstadt, Germany). Horse heart apomyoglobin (apo-Mb) was prepared according to the acid/acetone method (8) and the quality of preparation was tested by a 1:1 hemin titration.

Methods

Circular dichroism spectroscopy

CD spectra were measured at 20°C on a JASCO J-710 spectrometer (JASCO Spectroscopic, Hachioji, Japan) using a cell with a path length of 0.2 cm (in the far-ultraviolet (UV) region) and of 1.0 cm (in the Soret and the near-UV region). Data were collected every 0.2 nm with 1-nm bandwidth, at a scan speed of 50 nm/min. CD spectra are averages of four scans. Molar ellipticity $[\theta]$ (deg/cm^2/dmol^{-1}) is expressed on a mean residue concentration basis in the far-UV and on a protein concentration basis in the near-UV and Soret region.

Resonance Raman spectroscopy

RR spectra were obtained by excitation with the 406.7- and 413.1-nm lines of a Kr^+ laser (Coherent, Innova 90/K, Santa Clara, CA). The back-scattered light from a slowly rotating NMR tube was collected and focused into a computer-controlled double monochromator (Jobin-Yvon HG 2S, Villeneuve d'Ascq, France) equipped with a cooled photomultiplier (RCA C31034 A) (Burle Industries, Baesweiler, Germany) and photon-counting electronics. The spectral resolution was 5 cm^{-1}. The RR spectra were calibrated to an accuracy of ± 1 cm^{-1} for intense isolated bands, with indene as standard for the high-frequency region and with both indene and CCl_4 for the low-frequency region. Polarized spectra were obtained by inserting a Polaroid analyzer between the sample and the entrance slit of the monochromator. The depolarization ratios, $\rho = I_\perp/I_\parallel$, of the bands at 314 and 460 cm^{-1} of CCl_4 were measured to check the reliability of the polarization measurements. The values obtained, 0.73 and 0.00, respectively, compare well with the theoretical values of 0.75 and 0.00, respectively.

Stopped-flow kinetics

Stopped-flow experiments were carried out on an SX.18MV stopped-flow microanalyzer (Applied Photophysics, Leatherhead, UK), provided with a diode array, in a thermostatically controlled sample-handling unit at 25°C. The reaction was followed by collecting transient absorption spectra and then eventually converting this information to an appropriate single wavelength progress curve after mixing 1:1 v/v of SDS (at varying concentrations) with Mb (3 μM heme final concentration). We have followed the time course up to 200 s, but no further events were observed after 10 s. Moreover, the solution appeared stable without any apparent precipitation. Typically at least five runs were averaged at each SDS concentration to increase the signal/noise ratio. The data analysis for determination of apparent rate constants was carried out employing the Bateman approximation (9), as follows

$$OD_{\text{obs}} = OD_\infty \pm \sum_{i=1}^{i=n} \Delta OD_i \times \exp^{(-k_i \times t)_i}, \qquad (1)$$

where OD_{obs} is the observed optical density at a given wavelength, OD_∞ is the optical density at the end of the observation, ΔOD_i is the optical density change for the ith step, k_i is the rate constant for the ith step, and t is the time; the $\pm$ sign simply indicates that according to the wavelength the optical density can increase or decrease. This analysis provided both the amplitudes and rate constants associated with each relaxation phase. Subsequently, the data from two separate series of measurements were averaged.

Computer simulation

Computer simulation of the kinetic mechanism for the interaction of Mb with SDS was carried out using a second-order Runge-Kutta algorithm, calculating the individual populations of the Scheme in Fig. 7 at different time intervals (spaced by $dt = 0.1$ ms) and accounting for all forward and backward reactions involving each individual species. Values of rates are arbitrary and they have only a descriptive meaning, aiming to illustrate the behavior of such a reaction mechanism under conditions similar to those employed for experiments. In particular, for total concentrations of [SDS] < 4 mM, the micellar concentration $[SDS_m] = 0$, whereas for total concentration of [SDS] > 4 mM, the monomer concentration $[SDS_s] = 4$ mM and $[SDS_m] = [SDS] - 4$ mM.

RESULTS

Circular dichroism

To provide more insight into the structural transitions which Mb undergoes in the presence of SDS, we start with an analysis using CD and RR spectroscopy. This provides a useful background for the further description of the transitions observed by kinetic measurements.

The CD spectrum of a heme protein in the near-UV (250–350 nm) and Soret (350–450 nm) regions reflects changes in the protein tertiary structure that affect the environment of aromatic side chains and the heme pocket, respectively. Since the transitions giving rise to the bands in these regions are well characterized, the investigation of variations of their rotatory strength significantly helps in the interpretation of the conformational changes induced by SDS.

Fig. 1 shows the 250–500 nm CD spectra of Mb and of its imidazole complex (panel *A*) and of Mb upon gradual addition of SDS (panel *B*). The spectrum of Mb in the absence of SDS, in agreement with the results reported previously (10–13), is characterized in the Soret region by a positive band at 407 nm. In the presence of increasing concentrations of SDS, the positive band fades out with the concomitant appearance of a new negative red-shifted band at 421 nm. This transition is complete at [SDS] $\approx$ 2 mM. This is in agreement with the electronic absorption spectra (5), suggesting the formation of a bis-histidyl 6cLS heme upon addition of SDS. However, it must be emphasized that the CD spectrum of the complex between Mb and imidazole (panel *A*, trace (—)), which is also a bis-histidyl 6cLS complex, is fairly different from that of the Mb/SDS complex, since the former is characterized by a positive band at 416 nm. The negative band in the 300–350 nm region is due to imidazole, whereas the positive intense band at 259 nm is due to the overlap of the aromatic amino acids bands and a band due to the interaction between the heme and the protein. Its intensity has been correlated with the total magnetic moment (14). The opposite sign of the CD Soret band clearly indicates that the exogenous imidazole coordinated to the heme iron in the 6cLS Mb-imidazole complex and the histidine residues in the 6cLS Mb/SDS complex have largely different orientations. Further addition of SDS to 7 mM and to 100 mM brings about the disappearance of the ellipticity

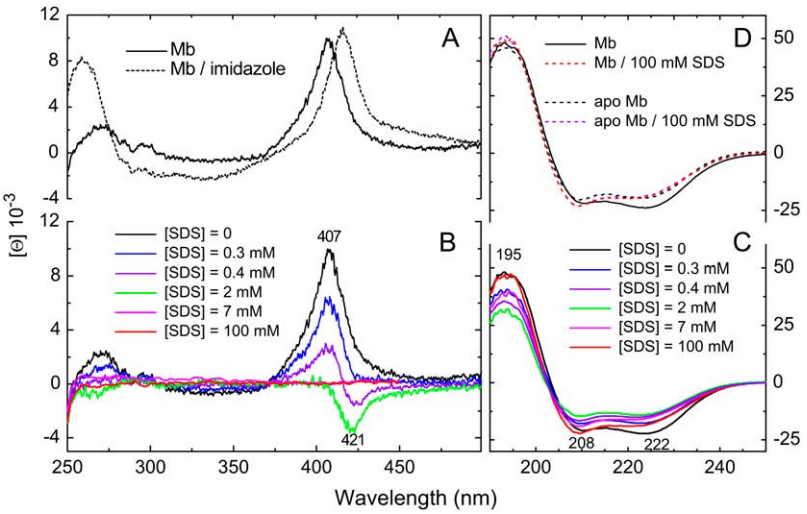

FIGURE 1 CD spectra (250–500 nm range) of (*A*) Mb (—) and Mb/imidazole complex (- - - -), and (*B*) Mb upon gradual addition of SDS. (*C*) CD spectra (190–250 nm range) of Mb upon gradual addition of SDS. (*D*) Comparison of the CD spectra of Mb and apo-Mb with and without 100 mM SDS.

in the Soret region. The corresponding absorption spectra (5) suggest that this phenomenon must be attributed to different events at 7 mM and at 100 mM SDS. The absorption spectrum at 7 mM SDS was assigned to an HS species whose coordination state could not be characterized, whereas the spectrum at 100 mM SDS was ascribed to the detachment of heme from the protein (i.e., free heme). Unfortunately, the CD spectra cannot discriminate between these HS species, even though the absence of signals in the Soret region indicates an achiral environment in both cases.

In the UV region, a reduction in intensity of the 208–222-nm dichroic bands is observed up to 2 mM SDS that is accompanied by a decrease of ellipticity at 195 nm (panel *C*). An intensity decrease of these bands indicates a reduction of the α-helix content (15), in accord with previous results (16). Furthermore, the relative magnitudes of the minima at 208 and 222 nm shift from $\theta_{222}/\theta_{208} > 1$ (no surfactant) to $\theta_{222}/\theta_{208} < 1$ (in the presence of surfactant). Such changes are indicative of the dissociation of α-helices from each other to form separate structural units (17) and of the rearrangement of aromatic residues due to the decreased rigidity of the tertiary structure. These groups contribute to a different extent to the change of the CD spectrum in the far-UV region with respect to the native state (18).

Upon increasing the SDS concentration over the range in which micellar formation occurs, a different behavior is observed (panel *C*). The ellipticity at 195 nm is recovered and it increases in the 208–222 nm region, even though a $\theta_{222}/\theta_{208} < 1$ is always observed. Interestingly, in the presence of 100 mM SDS the CD spectra of Mb and apo-Mb are identical in the UV region (panel *D*). On the other hand, the spectrum of apo-Mb in the absence of surfactant shows a lesser degree of ellipticity than the corresponding spectrum of Mb. This result is consistent with the separation of heme from Mb at 100 mM SDS, leading to the disappearance of ellipticity in the Soret region and to the appearance of the apo-Mb spectrum in the UV region.

Resonance Raman spectroscopy

RR spectroscopy has been extensively applied to heme proteins (19), since it provides information on the coordination and spin state of the heme iron. Therefore, we have performed a thorough RR analysis in the highly informative spectral region from 1300 to 1700 cm^{-1}. Fig. 2 shows the RR spectra of Mb and its imidazole complex (*A*) and of Mb upon addition of SDS (*B*).

The RR spectrum of ferric Mb (Fig. 2 *A*, trace —) has the features of an aquo six-coordinated high-spin (6cHS) heme (1482 (ν_3), 1513 (ν_{38}), 1544 (ν_{11}), 1563 (ν_2), 1582 (ν_{37}) cm^{-1}). Moreover, the intense band at 1621 cm^{-1} is due to the two vinyl $\nu_{(C=C)}$ stretching modes (20). Upon addition of imidazole (Fig. 2 *A*, trace—) the spectral changes indicate the formation of a 6cLS heme (1505 (ν_3), 1550 (ν_{38}), 1562 (ν_{11}), 1580 (ν_2), 1601 (ν_{37}), 1641 (ν_{10}) cm^{-1}). No frequency change is observed for the vinyl $\nu_{(C=C)}$ stretching band. The RR spectrum of Mb in the presence of 1 mM SDS is fairly similar to that observed for the Mb-Im complex (1505 (ν_3), 1548 (ν_{38}), 1562 (ν_{11}), 1579 (ν_2), 1601 (ν_{37}), 1641 (ν_{10}) cm^{-1}). The only difference is observed in the vinyl-stretching region, since two bands at 1621 and 1632 cm^{-1} are observed. These bands are assigned to two vinyl $\nu_{(C=C)}$ stretching modes on the basis of the polarized spectra (Fig. 2 *B*, //, trace—, $\perp$, trace ···), their depolarization ratio being $\rho = 0.14$ and $\rho = 0.27$, respectively, as determined by a curve-fitting analysis (data not shown). The ratio for the 1641 cm^{-1} band was $\rho = 0.89$. If the large overlap of these bands is considered, the depolarization ratios favorably compare with the theoretical values, $0.125 < \rho < 0.33$ (21) and $\rho = 0.75$ (20), expected for the vinyl and the ν_{10} mode, respectively.

The presence of two vinyl bands in the RR spectra in Fig. 2 *B*, compared to the single band in Fig. 2 *A*, is particularly interesting. A direct relationship between the $\nu_{(C=C)}$ stretching frequency and the orientation of the vinyl groups, as induced by specific protein interactions, has recently been

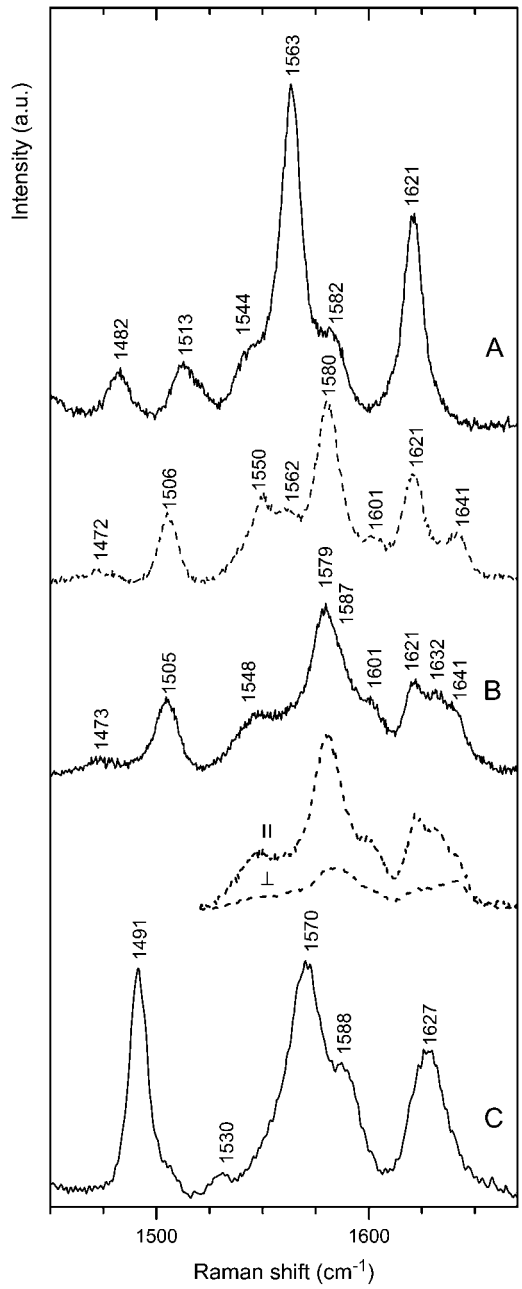

FIGURE 2 RR spectra of (*A*) Mb (—) and Mb/imidazole complex (—). Experimental conditions: 20 mW laser power; λ_{exc}.406.7 nm, 1 s/0.5 cm^{-1} accumulation time (—), λ_{exc}.413.1 nm, 4 s/0.5 cm^{-1} accumulation time (—); (*B*) Mb in the presence of 1 mM SDS; 40 mW laser power, λ_{exc}.413.1 nm, 9 s/0.5 cm^{-1} accumulation time; the polarized spectra were measured with 5 s/0.5 cm^{-1} (//) and 24 s/0.5 cm^{-1} accumulation time (⊥); (*C*) Mb in the presence of 100 mM SDS; λ_{exc}.406.7 nm, 40 mW laser power, 8 s/0.5 cm^{-1} accumulation time.

found in heme-containing peroxidases (22). In particular, it was found that when the protein matrix exerts no constraint on the vinyl groups, the latter take the torsional conformation usually found in model compounds in solution (23), and two $\nu_{(C=C)}$ stretching modes should be observed in the RR spectrum. Hence, we suggest that the presence of two distinct vinyl-stretching bands in the RR spectra of Mb in 1 mM SDS solution is related to a reduced steric hindrance of one of the two vinyls caused by the protein conformational change which accompanies the formation of the 6cLS species.

Upon increasing [SDS], a five-coordinated high-spin (5cHS) species increases at the expense of the 6cLS, as clearly shown in Fig. 2 *C*, which shows the RR spectrum of Mb in the presence of 100 mM SDS (1491 (ν_3), 1530 (ν_{38}), 1570 (ν_2), 1588 (ν_{37}), 1627 (overlapping ν_{10} and $\nu_{(C=C)}$) cm^{-1}). Since the 5cHS heme complex at high [SDS] is likely due to the detachment of heme from the protein and solvation into surfactant micelles, it is not surprising that the RR spectrum in Fig. 2 *C* is identical to that of hemin in the presence of SDS (23).

Time-resolved spectroscopic studies

When Mb is mixed with SDS, a minimum of ~0.1 mM surfactant is needed to elicit spectroscopic changes with time. Above this concentration level, we observe different spectral evolutions at different concentration ranges (Fig. 3), suggesting the occurrence of more than one pathway after the interaction of Mb with SDS. This becomes evident also for single wavelength progress curves (Fig. 4).

In particular, at the lowest [SDS] (0.5 mM, Fig. 3 *A*), the spectra display a simple evolution from the initial state of Mb, with maxima at 409, 505, and 639 nm, to a final state with maxima at 414, 535, and 567 nm, and no charge transfer band (CT1) in the 600–650 nm region. Thus, this final state corresponds to the bis-histidyl, 6cLS species, which is observed in the steady-state absorption spectra between 0.2 and 1 mM [SDS] (5) and which has also been characterized by the CD spectra in Fig. 1 *B* and the RR spectra in Fig. 2 *B*. In the presence of 2 mM SDS (Fig. 3 *B*) the absorption spectra change in a very similar way. The conversion from the initial state of Mb to the 6cLS form occurs faster and is complete within 70 ms. A different absorption spectral evolution occurs at 7 mM [SDS] (Fig. 3 *C*). After the fast conversion to the 6cLS form, a new species appears at 70 ms with distinct maxima at 410 nm (Soret band) and 628 nm (CT1 band). The spectral features of this species are essentially the same as those of the HS species, which is observed at the steady state at 7 mM [SDS] (5), but distinct from those of protein-free heme. Notably, the new species, which we will indicate as $(HS)_I$, is partially converted to the 6cLS form after some seconds. At higher SDS concentrations (i.e., [SDS] > 10 mM), the kinetic pattern undergoes a further change, which is documented at 100 mM [SDS] in Fig. 3 *D*. The evolution of the absorption spectra leads to the appearance of a species with maxima at 400 nm (Soret band), 492 nm (β band), and 609 nm (CT1 band). This is the well-known spectrum of heme in SDS micelles, which has been studied by the combination of several spectroscopic methods (24).

Therefore, looking at kinetic progress curves at a given wavelength (e.g., 414 nm, see Fig. 4 *A*), the number of

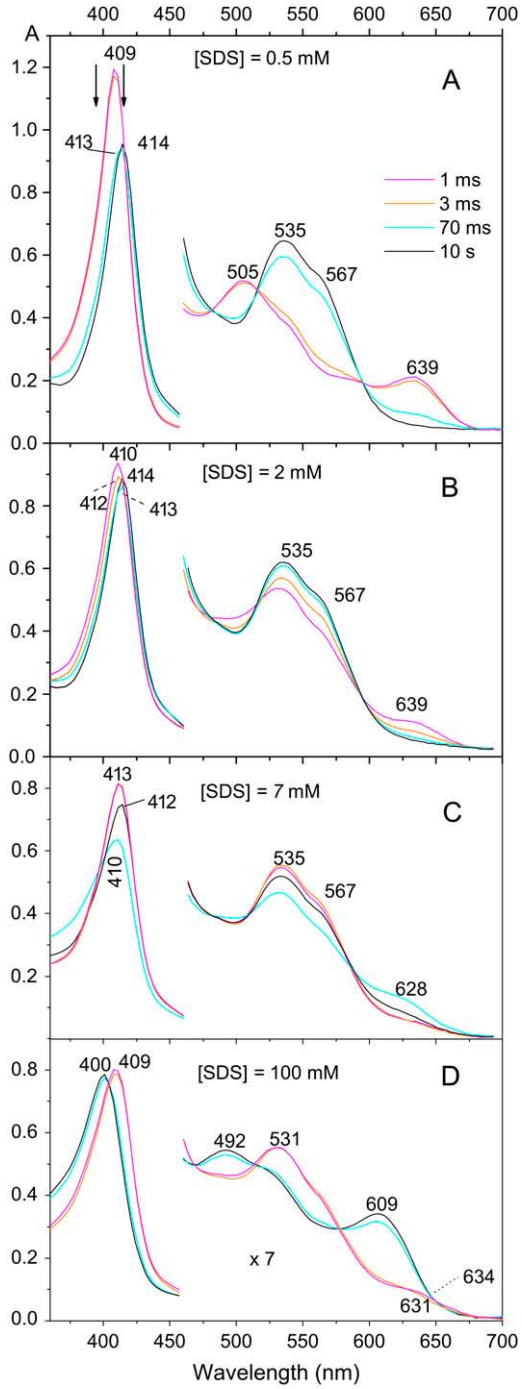

FIGURE 3 Time-resolved absorption spectra of Mb in the presence of increasing SDS concentrations, namely, 0.5 mM (*A*), 2 mM (*B*), 7 mM (*C*), and 100 mM (*D*) . Absorption spectra in the visible range are enhanced sevenfold to compare spectral variations in the Soret and in the visible region. The two arrows in the highest panel mark the detection wavelengths (414 and 395 nm) for the kinetic curves shown in Fig. 4.

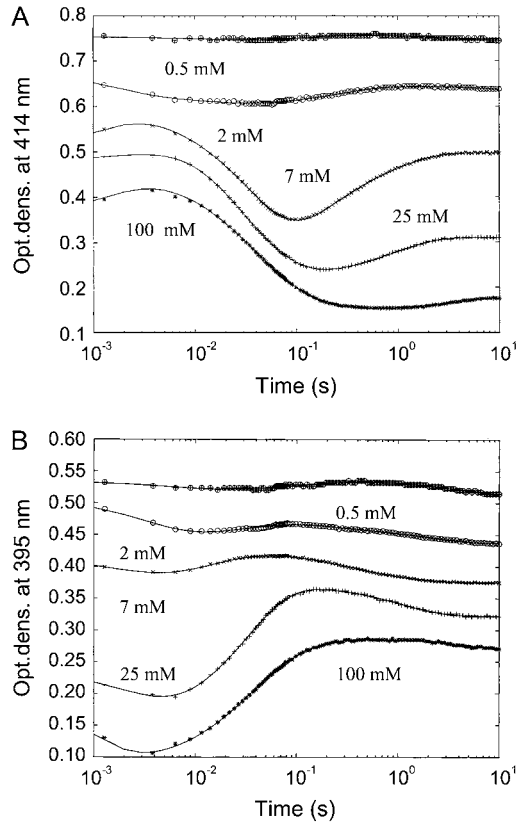

FIGURE 4 Kinetic progress curves at (*A*) 414 nm and (*B*) 395 nm at different SDS concentrations, namely 0.5 mM (⊕), 2 mM (o), 7 mM (x), 25 mM (+), and 100 mM (*). Continuous lines are nonlinear least-squares fitting of data according to Eq. 1.

relaxation phases seems to vary with SDS concentration, even though for homogeneity we have analyzed all traces with four exponentials, obviously obtaining different amplitudes for various phases at different SDS concentrations. As a matter of fact, up to 2 mM [SDS] we observe mostly three phases; whereas between 2 and 10 mM [SDS] a fourth phase rises up, at the expense of another one, becoming predominant at higher SDS concentrations. Therefore, from a phenomenological viewpoint, kinetic progress curves could be described reasonably well with only three phases below 2 mM [SDS] and above 10 mM [SDS], whereas at intermediate SDS concentrations curve fitting indeed requires a fourth exponential. The rate constants and amplitudes obtained from the fitting are plotted in Fig. 5 as a function of [SDS]. We term the four phases as the very fast, fast, intermediate, and slow phase, respectively, and we describe them in more detail in the following.

Very fast phase

This phase can be observed well only at the lowest SDS concentrations, but the tail of the exponential can be detected at all concentrations. Both its amplitude and its rate display a marked dependence on [SDS] (Fig. 5 *A*). The sign of the amplitude at 414 nm is different according to whether [SDS] $\leq$ 2 mM or not (see Fig. 4 *A*). On the other hand, at 395 nm the amplitude sign seems independent of [SDS]. Therefore, we have chosen to report in Fig. 5 *A* the dependence on

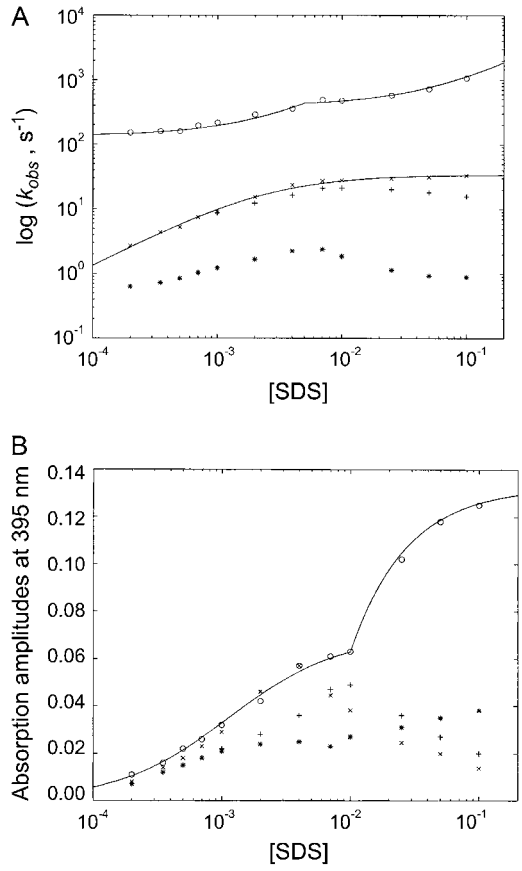

FIGURE 5 Dependence on SDS concentration of (*A*) rate constants and (*B*) absorption amplitudes for the very fast phase (o), the fast phase (x), the intermediate phase (+), and the slow phase (*). Values for rate constants (k_{obs}) refer to those obtained at 395 nm (closely similar to those obtained at 414 nm), except for the data of the intermediate phase, whose values correspond to those obtained at 414 nm. All absorption amplitudes correspond to those obtained at 395 nm. Continuous line in panel *A* is the nonlinear least-squares fitting of data according to Eq. 2, accounting for the fact that at [SDS] $\geq$ 4 mM the contribution to the observed k_{ff} comes also from micellar SDS. Resulting parameters are the following: (solution SDS) $k_{on} = 5.3$ ($\pm$0.6) $\times$ 10^4 $M^{-1}s^{-1}$, $k_{off} = 60$ ($\pm$8) s^{-1}; (micellar SDS) $k_{on} = 7.4$ ($\pm$0.9) $\times$ 10^3 $M^{-1}s^{-1}$, $k_{off} = 75$ ($\pm$9) s^{-1}. The continuous line in panel *B* simply corresponds to the expected absorption amplitude on the basis of the equilibrium constants for Mb interaction with solution and micellar SDS, derived from the fitting reported in panel *A*, employing a $\Delta OD = 0.07$ for the interactions of Mb with both solution and micellar SDS.

[SDS] of the rate constants determined at 395 nm (which are similar to those observed at 414 nm). Interestingly, this dependence shows a bimodal behavior, as if there are two distinct processes corresponding to the SDS bimolecular interaction with Mb. The same is true for the absorption amplitude of the process, reinforcing the idea that two very fast events are taking place. Since the discontinuity occurs at concentrations close to 4 mM, i.e., the cmc of Mb/SDS, we can postulate that the two processes reflect the two different states of SDS (monomeric and micellar), which interact with Mb with different rate constants. The concentration dependence of the rate constants, k_{ff}, for each state can then be analyzed according to a simple linear relationship

$$k_{ff} = k_{on} \times [SDS] + k_{off}, \quad (2)$$

where k_{ff} is the observed rate constant for the very fast phase, k_{on} is the bimolecular association rate constant, and k_{off} is the dissociation rate constant. We must distinguish between the concentration of monomeric SDS, [SDS_s], and that of micellar SDS, [SDS_m], since [SDS_s] never exceeds 4 mM, whereas at higher total [SDS] only [SDS_m] increases. The continuous line in Fig. 5 *A* takes into account this behavior, and the breaking point refers to the coming into play of micellar SDS. The resulting values are i) for monomeric SDS $k_{on} = 5.3 \times 10^4$ M^{-1} s^{-1} and $k_{off} = 60$ s^{-1}, and ii) for micellar SDS $k_{on} = 7.4 \times 10^3$ M^{-1} s^{-1} and $k_{off} = 75$ s^{-1}. Furthermore, it is interesting to outline that for this phase, we can describe the amplitude, employing the equilibrium constants for the binding of Mb to monomeric SDS ($k_{on}/k_{off} = 8.83 \times 10^2$ M^{-1}) and to micellar SDS ($k_{on}/k_{off} = 9.87 \times 10^1$ M^{-1}), again accounting for the appearance of micellar SDS at the critical concentration, which corresponds to the discontinuity in the continuous curve in Fig. 5 *B*.

Fast phase

For the fast phase, the observed rate constant, k_{fast}, displays a dependence upon [SDS] (Fig. 5 *A*), which, however, levels off at [SDS] $>$ 10 mM with a limiting value of $\sim$35 s^{-1}. Also, for the absorption amplitude of this process we observe a peak value at the same SDS concentration range, decreasing as [SDS] further rises up. This behavior clearly indicates that this fast phase is referable to a unimolecular process (likely a conformational change after the binding of SDS to Mb), and the observed concentration dependence simply reflects an incomplete saturation degree of Mb by SDS. Therefore, as a whole the very fast phase (i.e., SDS binding) and the fast phase can be analyzed in terms of a preequilibrium (with $k_{off} > k_{fast}$) followed by a unimolecular process, which is concentration dependent as long as Mb is not fully saturated by SDS, as in the following scheme:

$$Mb_N + SDS \xleftrightarrow{K_{SDS}} Mb_N : SDS \xrightarrow{k_d} Mb_A : SDS \quad \text{(Scheme1)}$$

where Mb_N and Mb_A denote the native and (partially) unfolded state of Mb, $K_{SDS} = [Mb_N][SDS]/[Mb_N{:}SDS] = k_{off}/k_{on}$ is a preequilibrium corresponding to the very fast phase described above, and k_d is the rate constant for the conformational change after binding. Note that we do not imply that Mb_A is completely unfolded, but it must have undergone some structural change relative to Mb_N. The data fit reasonably well to Eq. 3, which accounts for the overall process

$$k_{fast} = k_d \times \frac{[SDS]}{K_{SDS} + [SDS]}. \quad (3)$$

The continuous line in Fig. 5 *A* for the fast phase is obtained, employing Eq. 3 with $k_d = 35$ s^{-1} and $K_{SDS} = 60/$

$5.3 \times 10^4 = 1.13 \times 10^{-3}$ M, as obtained from the fitting of the very fast phase to Eq. 2. The fact that k_{fast} levels off at SDS concentrations which are close to the cmc indicates that the fast phase mostly concerns SDS monomers rather than bulk micelles.

Intermediate phase

For the intermediate phase, which can be observed clearly only between 1 and 10 mM [SDS] (displaying the formation of the HS_I species, see Fig. 3 *C*), we report the values of rate constants obtained at 414 nm, since the third intermediate phase is observed much better at this wavelength, where it displays an amplitude sign opposite to that of the second fast phase. This is very important, since the rate constants for the second and the third phase are fairly similar and not easily distinguishable at 395 nm (see Fig. 4 *B*). The rate constant, k_{int}, also seems to increase as a function of SDS concentration from $\sim$10 s^{-1} at 2 mM SDS to $\sim$25 s^{-1} at 10 mM (see Fig. 5 *A*); and the same can be observed for the absorption amplitude (see Fig. 5 *B*), which, however, decreases at higher SDS concentration, keeping a closely similar value of the rate constant (see Fig. 5 *A*). In this case, as well as for the slow rate, we did not try to quantitatively fit the data, since the system becomes so complex that fitting parameters would have no definite physical meaning.

Slow phase

This process, which leads to different final species according to the SDS concentration regime (i.e., mostly 6cLS forms at [SDS] $\leq$ 10 mM and predominantly free heme at [SDS] $\geq$ 20 mM, see Fig. 3 *D*), is characterized by a rate constant somewhat dependent on SDS concentration (Fig. 5 *A*) up to 5 mM [SDS] (likely referring to the formation of the final 6cLS form). At higher [SDS] the apparent rate constant (likely referring to the formation of the free heme) displays lower values. The absorption amplitude of the process, which increases up to 5 mM [SDS], remains constant between 5 mM [SDS] and 10 mM [SDS], then further increases (see Fig. 5 *B*). This behavior seems to reflect the fact that i) the first increase corresponds to the formation of the final 6cLS form in the presence of the monomeric SDS, whereas ii) the second increase corresponds to the formation of the free heme.

DISCUSSION

Different modes of protein-surfactant interactions have been reported for various kinds of protein/surfactant complexes (25–27). In the case of the interaction of Mb with SDS we observe a complex process both from the static and from the dynamical points of view. The combination of the different steady-state spectroscopies—absorption, CD, and RR—and the comparison between the UV CD spectra of apo-Mb and Mb at 100 mM [SDS] (Fig. 1 *D*) allow us to make a first separation between two events occurring in the process: a moderate conformational change in the tertiary structure, leading to the formation of a 6cLS heme, and a real unfolding, which brings about the detachment of heme from the protein matrix. The kinetic measurements are consistent with this dual protein-surfactant interaction and yield additional information about intermediate steps which are not evident in the stationary observations. Depending on SDS concentration, we observe three or four relaxation phases during the interaction of Mb with SDS. It is clear that there are three general concentration regimes, namely 0.1–1 mM, 1–10 mM, and 10–100 mM SDS (Figs. 4 and 5). We discuss the events occurring in each of the three regimes separately.

The 0.1–1 mM SDS regime

The spectroscopic data at equilibrium have shown that over this concentration range the formation of a 6cLS species is the main event occurring at the heme cavity. Consistently, the time-resolved absorption spectra (Fig. 3 *A*) display the change from the initial (6cHS aquo) Mb state to the 6cLS form. As anticipated in the Results section, the interaction of Mb with SDS appears to involve the surfactant in its monomeric form.

The 1–10 mM SDS regime

In the second regime, we also observe the final formation of a 6cLS form (see Fig. 3, *B* and *C*), but we can detect the appearance of the intermediate form, HS_I (which becomes more evident as [SDS] rises from 2 mM to 7 mM, see Fig. 3 *C*). As a consequence, the amplitudes for the fast and the intermediate phases display opposite signs at 414 nm (see Figs. 3 *C* and 4 *A*). This complex kinetics is consistent with the steady-state absorption spectra, where an equilibrium between the 6cLS and the $(HS)_I$ species appears in this SDS concentration range. Unfortunately, the $(HS)_I$ intermediate can be scarcely characterized by steady-state techniques, since i), its absorption spectrum overlaps with those of the other Mb forms, ii), its heme appears to be achiral, and iii), its RR bands are also overlapped with those of both the 6cLS form and of protein-free heme. However, time-resolved absorption spectra at 7 mM [SDS] (Fig. 3 *C*) yield the important evidence that the $(HS)_I$ species indeed is an intermediate in the formation of the 6cLS species. As a matter of fact, it builds up during the first 70 ms after the mixing of Mb with SDS, and it is slowly converted to the 6cLS form in a few seconds (see Figs. 3 *C* and 4).

The 10–100 mM SDS regime

Both steady-state and time-resolved absorption spectra (for delays >70 ms) display the features of an HS species which can be identified as protein-free heme.

We summarize the steady-state spectroscopic data, the time-resolved data, the transient spectra, and the tensiometry data from Tofani et al. (5) in a scheme which implies the existence of two modes of interaction of Mb with SDS according to whether it is monomeric or micellar (Fig. 6). According to this reaction mechanism, Mb reacts with monomeric SDS in solution $(SDS)_s$ and/or with SDS micelles $(SDS)_m$. The two pathways are separated but are interconnected, since $[SDS_s]$ is always $\leq$4 mM and for higher SDS concentrations only $[SDS_m]$ increases; therefore, at [SDS] $\geq$ 4 mM we have both forms of SDS, which interact with Mb at different bimolecular rate constants. We also note that $[SDS_s]$ should be constant in the range 0.37–2 mM due to the formation of protein-surfactant aggregates, according to the tensiometric data (5). On the other hand, there are no evident effects of this process on the kinetic parameters.

It must be remarked that the bimolecular complexes (i.e., species (1) and (5) in Fig. 6) do not imply an interaction of SDS with the heme iron. This statement seems supported by the clear-cut differences between the Mb/SDS complex and Mb/imidazole complex (see Figs. 1 and 2). In this respect, it may be worth recalling the presence of several positively charged residues in the immediate vicinity of the distal side of the heme pocket, namely i), Lys-62 and Lys-63 (thus adjacent to the distal His-64); and ii), Lys-77, Lys-78, and Lys-79, which also belong to the E helix and may form salt bridges with Glu-18 (helix A) (28), Glu-85 (helix F), and Asp-4 (helix A) (29). As a whole, these interactions will certainly bring about the rupture of salt bridges with a consequent alteration of the structural arrangement of the distal side of the heme pocket, with consequently much larger flexibility of the E helix, which would then favor the formation of the 6cLS form by the axial coordination of the distal His-64.

Further, it must be underlined that the formation of the intermediate species in the range between 1 mM SDS and 10 mM SDS should belong to the pathway involving the interaction between Mb and monomeric SDS, since its relevance decreases as the second pathway comes into play when [SDS] $\geq$ 10 mM (i.e., when the interaction between Mb and micellar SDS becomes predominant). Therefore, within the pathway after the interaction of Mb with monomeric SDS (see Fig. 6), we have introduced an additional alternative bimolecular process between monomeric SDS and Mb (likely involving indirectly the heme-binding site), which brings about the formation of an intermediate species which must then be identified as the intermediate HS_I species observed at 7 mM SDS (see Fig. 3 *C*). Also in this case, the SDS interaction does not involve the heme iron and it is likely due to the positive cluster of lysine residues mentioned above.

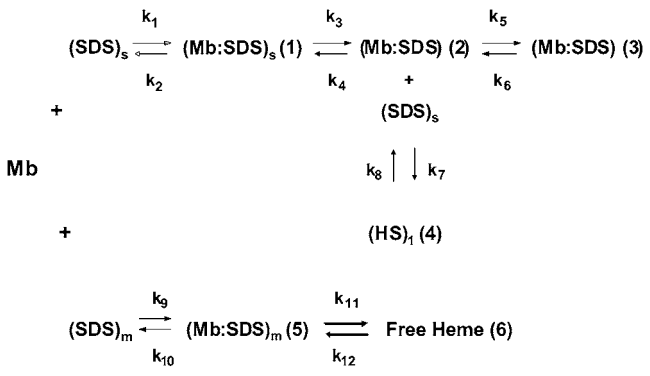

FIGURE 6 Proposed mechanisms for the interaction between Mb and SDS.

On the other hand, the interaction of Mb with micellar SDS (i.e., the *left* side pathway in Fig. 6) may be much simpler, leading to an interaction of micellar SDS with Mb that brings about a much more drastic structural alteration of the protein, which likely unfolds completely, and the consequent detachment of the heme from the protein matrix. The expected behavior of this scheme is simulated in Fig. 7 for a given set of kinetic parameters at different SDS concentrations, reporting the time dependence of concentration for various species represented in Fig. 6. Obviously, the behavior reported in Fig. 7 is only a general indication of possible kinetic scenarios; the curves do not follow experimental points and, therefore, they do not mean to represent a unique description of the system. The main aspect with reference to the data reported above is the fact that whereas at high (i.e., $\geq$10 mM) SDS concentration and at low (i.e., $\leq$ 1 mM) SDS concentration the temporal evolution of species shows a triphasic time course, at intermediate (i.e., 7 mM) concentrations there is a tetraphasic time course (see Fig. 4). This is due to the fact that, as [SDS] rises up, the second bimolecular step (leading to species (4) in Fig. 6) comes more and more into play (see Fig. 7). Its relevance is reduced with the predominant binding of micellar SDS at higher SDS concentrations.

The existence of a third independent pathway can be ruled out on the basis of observations by sequential mixing experiments (data not shown), since Mb first exposed to intermediate SDS concentrations for a given aging time and then to a second final concentration was always able to attain the same final species independent of the SDS exposure history.

From data reported in Fig. 5 *A*, where a nonlinear least-squares fitting of rate constants for the first bimolecular steps has allowed us to determine the binding rate constants to Mb of monomeric and micellar SDS (i.e., k_1, k_2, k_9, and k_{10}), we observe that the interaction is kinetically and thermodynamically more favorable for the monomeric SDS, rendering the upper pathway in Fig. 6 preferential also at intermediate [SDS]: this is the reason we have been forced to imply that the formation of the $(HS)_I$ species at intermediate [SDS] belongs to the upper pathway in Fig. 6. In practice, because of the relative values of k_1, k_2, k_7, k_8, k_9, and k_{10} (see Fig. 6), we have the following mechanisms at different SDS regimes:

- 0.1–1 mM SDS: the preferential pathway goes through species (1), (2) to (3);
- 1.0–10 mM SDS: the preferential pathway goes through species (1), (2) to (4) (driven by kinetics), which

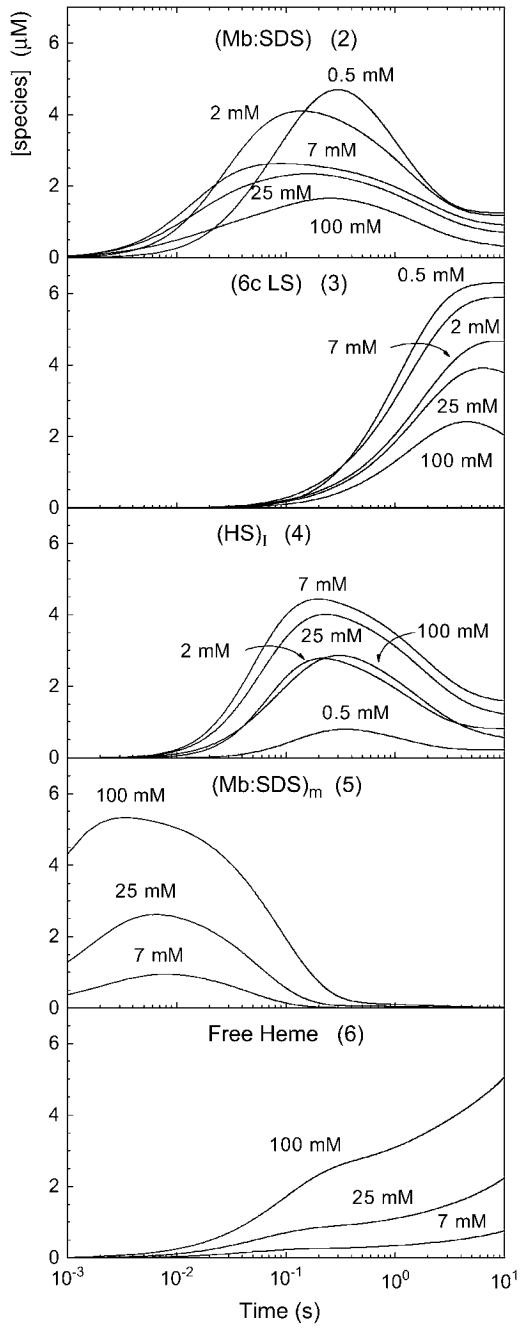

FIGURE 7 Time evolution of the concentration of the species from (2) to (6) in the scheme reported in Fig. 6. Each panel displays the time evolution for each of the five species at 0.5, 2, 7, 25, and 100 mM [SDS]. The parameters employed for describing the behavior of the system are $k_1 = 5.3 \times 10^4\ M^{-1}\ s^{-1}$, $k_2 = 60\ s^{-1}$, $k_3 = 35\ s^{-1}$, $k_4 = 2\ s^{-1}$, $k_5 = 1\ s^{-1}$, $k_6 = 0.2\ s^{-1}$, $k_7 = 8.7 \times 10^3\ M^{-1}s^{-1}$, $k_8 = 25\ s^{-1}$, $k_9 = 7.4 \times 10^3\ M^{-1}s^{-1}$, $k_{10} = 75\ s^{-1}$, $k_{11} = 5\ s^{-1}$, $k_{12} = 0$.

slowly reequilibrates to give species (3) through the formation of species (2);

10–100 mM SDS: the presence of micellar SDS opens the lower pathway in Fig. 6 (i.e., formation of free heme (6) through species (5)); and

10–100 mM SDS: the large predominance of micellar SDS over monomeric SDS renders the lower pathway in Fig. 6 (i.e., through species (5) and (6)) prevalent.

This is represented in Fig. 7, where each panel displays the time evolution for one of the five Mb species from (2) to (6) at increasing SDS concentrations. The interested reader can also compare Fig. 7 with the figure in the Supplementary Material, which presents the same data in a different way, showing the time evolution of all five Mb species at a given SDS concentration.

CONCLUSION

We have demonstrated that the interaction between Mb and SDS should not be viewed as a simple protein-ligand-binding process. The complexity observed in the steady-state spectra has its counterpart in the dynamics of the conformational changes induced in the protein by the surfactant. This can be regarded as a multipathway and multistep process, which we have consequently analyzed in the two dimensions of time and SDS concentration. The analysis has lead to a detailed scheme for the formation of Mb/SDS complexes which includes the stable species observed at equilibrium and additional reaction intermediates.

The complexity of this reaction might also be encountered in other biological systems, and we can expect that other proteins—and other surfactants—interact in a rather similar way.

SUPPLEMENTARY MATERIAL

An online supplement to this article can be found by visiting BJ Online at http://www.biophysj.org.

This work was funded by grants from the Italian Ministry of Education, University, and Research (MIUR) (PRIN) and the Università di Firenze (ex 60%) to G. S. and A. F. and from FIRB (RBNE03PX83) to M.C.

REFERENCES

1. La Mesa, C. 2005. Polymer-surfactant and protein-surfactant interactions. *J. Colloid Interface Sci.* 286:148–157.
2. Gohon, Y., and J.-L. Popot. 2003. Membrane protein surfactant complexes. *Curr. Opin. Colloid Interface Sci.* 8:15–22.
3. Oellerich, S., H. Wackerbarth, and P. Hildebrandt. 2003. Conformational equilibria and dynamics of cytochrome *c* induced by binding of sodium dodecyl sulfate monomers and micelles. *Eur. J. Biophys.* 32: 599–613.
4. Viseu, M. I., T. I. Carvalho, and S. M. B. Costa. 2004. Conformational transitions in β-lactoglobulin induced by cationic amphiphiles: equilibrium studies. *Biophys. J.* 86:2392–2402.
5. Tofani, L., A. Feis, R. E. Snoke, D. Berti, P. Baglioni, and G. Smulevich. 2004. Spectroscopic and interfacial properties of myoglobin/surfactant complexes. *Biophys. J.* 87:1186–1195.
6. Mikšovská, J., J. Yom, B. Diamond, and R. W. Larsen. 2006. Spectroscopic and photothermal study of myoglobin conformational changes in the presence of sodium dodecyl sulfate. *Biomacromolecules.* 7:476–482.

7. Antonini, E., and M. Brunori. 1971. Hemoglobin and Myoglobin in Their Reactions with Ligands. North Holland Publication, Amsterdam.
8. Ascoli, F., M. R. Rossi Fanelli, and E. Antonini. 1981. Preparation and properties of apohemoglobin and reconstituted hemoglobins. *Methods Enzymol.* 76:72–77.
9. Bateman, H. 1910. Solutions of certain partial differential equations. *Proc. Camb. Phil. Soc. Math. Phys. Sci.* 15:423–427.
10. Chen, Y.-H., J. T. Yang, and H. M. Martinez. 1972. Determination of the secondary structures of proteins by circular dichroism and optical rotatory dispersion. *Biochemistry.* 11:4120–4131.
11. Greenfield, N., and G. D. Fasman. 1969. Computed circular dichroism spectra for the evaluation of protein conformation. *Biochemistry.* 8: 4108–4116.
12. Holzwarth, G., and P. Doty. 1965. The ultraviolet circular dichroism of polypeptides. *J. Am. Chem. Soc.* 87:218–228.
13. Nicola, N. A., E. Minasian, C. A. Appleby, and S. J. Leach. 1975. Circular dichroism studies of myoglobin and leghemoglobin. *Biochemistry.* 14:5141–5149.
14. Kajiyoshi, M., and F. K. Anan. 1975. Conformation of biological macromolecules. Circular dichroism and magnetic circular dichroism studies of metmyoglobin and its derivatives. *J. Biochem.* (*Tokyo*). 78: 1087–1095.
15. Urry, D. W. 1967. The heme chromophore in the ultraviolet. *J. Biol. Chem.* 242:4441–4448.
16. Mattice, W. L., J. M. Riser, and D. S. Clark. 1976. Conformational properties of the complexes formed by proteins and sodium dodecyl sulfate. *Biochemistry.* 15:4264–4272.
17. Otzen, D. E. 2003. Folding of DsbB in mixed micelles: a kinetic analysis of the stability of a bacterial membrane protein. *J. Mol. Biol.* 330:641–649.
18. Manning, M. C., and R. W. Woody. 1989. Theoretical study of the contribution of aromatic side chains to the circular dichroism of basic bovine pancreatic trypsin inhibitor. *Biochemistry.* 28:8609–8613.
19. Spiro, T. G., and X. Y. Li. 1988. Resonance Raman spectroscopy of metalloproteins. *In* Biological Applications of Raman Spectroscopy, Vol. 3. T. G. Spiro, editor. Wiley, New York. 1–37.
20. Choi, S., T. G. Spiro, K. C. Langry, K. M. Smith, D. L. Budd, and G. N. La Mar. 1982. Structural correlations and vinyl influences in resonance Raman spectra of protoheme complexes and proteins. *J. Am. Chem. Soc.* 104:4345–4351.
21. DeVito, V. L., M.-Z. Cai, S. A. Asher, L. A. Kehres, and K. M. Smiths. 1992. UV resonance Raman evidence for vibrationally independent protoporphyrin IX vinyl groups. *J. Phys. Chem.* 96:6917–6922.
22. Marzocchi, M., and G. Smulevich. 2003. Relationship between heme vinyl conformation and the protein matrix in peroxidases. *J. Raman Spectrosc.* 34:725–736.
23. Kalsbeck, W. A., A. Ghosh, R. K. Pandey, K. M. Smith, and D. F. Bocian. 1995. Determinants of the vinyl stretching frequency in protoporphyrins. Implications for cofactor-protein interactions in heme proteins. *J. Am. Chem. Soc.* 117:10959–10968.
24. Boffi, A., T. K. Das, S. della Longa, C. Spagnuolo, and D. L. Rousseau. 1999. Pentacoordinate hemin derivatives in sodium dodecyl sulfate micelles: model systems for the assignment of the fifth ligand in ferric heme proteins. *Biophys. J.* 77:1143–1149.
25. Nielsen, A. D., L. Arleth, and P. Westh. 2005. Analysis of protein–surfactant interactions—a titration calorimetric and fluorescence spectroscopic investigation of interactions between *Humicola insolens* cutinase and an anionic surfactant. *Biochim. Biophys. Acta.* 1752: 124–132.
26. Otzen, D. E. 2002. Protein unfolding in detergents: effect of micelle structure, ionic strength, pH, and temperature. *Biophys. J.* 83:2219–2230.
27. Sun, C., J. Yang, X. Wu, X. Huang, F. Wang, and S. Liu. 2005. Unfolding and refolding of bovine serum albumin induced by cetylpyridinium bromide. *Biophys. J.* 88:3518–3524.
28. Evans, S. V., and G. D. Brayer. 1990. High-resolution study of the three-dimensional structure of horse heart metmyoglobin. *J. Mol. Biol.* 213:885–897.
29. Maurus, R., C. M. Overall, R. Bogumil, Y. Luo, A. G. Mauk, M. Smith, and G. D. Brayer. 1997. A myoglobin variant with a polar substitution in a conserved hydrophobic cluster in the heme binding pocket. *Biochim. Biophys. Acta.* 1341:1–13.